Antibacterial activity and structural characterization of Selenium nanoparticles synthesized from Cinnamon (*Cinnamomum zeylanicum*) bark extract

Fatima Ghazi Edem*

Ministry of Education, General Directorate of Education in Wasit, Iraq
*Corresponding author, email: fghazi1978@gmail.com

Article History
Received: 15 June 2026
Revised: 25 July 2026
Accepted: 20 August 2026

Keywords
Antibacterial activity
Cinnamomum zeylanicum
Green synthesis
Selenium nanoparticles
Staphylococcus aureus

Abstract
Selenium nanoparticles (SeNPs) have attracted attention due to their antioxidant and antimicrobial properties, but many synthesis methods still employ toxic reducing agents. This study developed a green, single-pot synthesis of SeNPs using aqueous cinnamon (Cinnamomum zeylanicum) extract as both reducing and capping agent, with ascorbic acid added to stabilize pH. A mixture of sodium selenite solution and 25 mL cinnamon extract was heated at 60–70 °C, producing a characteristic crimson-red color within 15 min, indicating elemental selenium formation. The nanoparticles were recovered by ethanol-induced precipitation and characterized using XRD, TEM, HRTEM, FTIR, and zeta potential analyses. XRD confirmed the trigonal selenium phase with an average crystallite size of 12.78 nm. TEM showed quasi-spherical particles with a mean diameter of 23.5 ± 4.8 nm, while HRTEM revealed a lattice fringe spacing of 0.34 nm. FTIR spectra indicated that polyphenols and aldehydic groups in the cinnamon extract participated in nanoparticle formation and stabilization. The colloid exhibited a zeta potential of −32.4 ± 4.21 mV, demonstrating good stability. Antibacterial activity was confirmed by disc diffusion assays, producing inhibition zones of 18.7 ± 1.2 mm against Staphylococcus aureus and 14.3 ± 1.0 mm against Escherichia coli ($p < 0.001$). These findings demonstrate that cinnamon-mediated SeNPs provide a stable, low-toxicity, and scalable platform for antibacterial applications.

How to cite: Edem, F, G. (2027). Antibacterial activity and structural characterization of Selenium nanoparticles synthesized from Cinnamon (Cinnamomum zeylanicum) bark extract. *Innovations in Science Education and Practice*, 4(1). 1-9. doi: 10.20961/t2tn4b34

1. Introduction

Selenium is one micronutrient that has a very small therapeutic window. It is located at the catalytic site of glutathione peroxidase and other selenoenzymes, which neutralize peroxide species and help to prevent oxidative damage to cell membranes (Papp, et al., 2007; Rayman, 2012). If this same element is engineered on the nanoscale, however, the activity profile changes in interesting ways: there is a large increase in surface area, increased redox behavior, and a decreased dose in which therapeutic benefit appears. Selenium nanoparticles (SeNPs) are thus being studied as antioxidants, antimicrobials, anticancer drug carriers, and supplements in functional food formulations (Wadhani, et al., 2016; Menon, et al., 2018; Khurana, et al., 2019).

Current methods of SeNP synthesis are still based on strong reducing agents like sodium borohydride, hydrazine hydrate, or formaldehyde. Although these reagents work, they do leave behind residue on the particle surface which makes them more difficult to use downstream in biomedical applications, and several of these reagents are acutely toxic and environmentally persistent (Tran & Webster, 2011). The physical method, such as laser ablation and γ-irradiation, does not leave any chemical residue, but it is expensive and only yields small amounts. In this context, biological synthesis paths have gradually become more and more popular. Plant-mediated approaches are especially appealing, due to their operational simplicity, use of aqueous media at moderate temperatures and their use of secondary metabolites that are both reductants and capping ligands (Iravani, 2011; Mittal, et al., 2013).

Cinnamon bark (*Cinnamomum zeylanicum*; also stated as C. verum) contains high levels of cinnamaldehyde, eugenol, coumarin, proanthocyanidins and a group of polyphenolic acids. The presence of the hydroxyl and aldehyde groups is well established as electron donors which can reduce metal ions, while the presence of hydrophobic groups allows physisorption at the

doi: 10.20961/t2tn4b34

ISSN: 3108-9097

nanoparticle surface and inhibits Ostwald ripening (Ranasinghe, et al., 2013; Sharma, et al., 2014). A few groups have already extracted Silver, Gold, Copper oxide and Zinc oxide nanoparticles from cinnamon and the materials obtained exhibit improved antimicrobial properties compared to the chemically synthesized ones (Husen & Siddiqi, 2014; Khiralla & El-Deeb, 2015). But there are relatively few reports on cinnamon-mediated SeNPs, and further elucidation of the relationship between structure and function is warranted.

The purpose of the present work is twofold. First, to obtain SeNPs through a low-energy route in which sodium selenite is reduced by an aqueous cinnamon extract, with ascorbic acid added as a mild pH buffer rather than as the principal reductant. Second, to characterise the as-prepared particles by XRD, FTIR, TEM, HRTEM, and zeta potential measurements, and to evaluate their inhibitory effect against one Gram-positive pathogen (*Staphylococcus aureus*) and one Gram-negative pathogen (Escherichia coli) using the standard disc-diffusion assay.

2. Materials and Method

2.1. Reagents and Plant Material

Sodium selenite (Na_2SeO_3, ≥ 98 %) and L-ascorbic acid (vitamin C, ≥ 99 %) were of analytical grade and used as received without further purification. Absolute ethanol was obtained from a commercial supplier. Distilled water was used throughout the experiments. Dried cinnamon (*C. zeylanicum*) bark, available locally as a culinary spice, was ground to a fine powder using a domestic mill and stored in a dry, dark glass container until use. The bacterial strains used in the antibacterial test, Staphylococcus aureus and Escherichia coli, were obtained from a clinical microbiology laboratory and maintained on nutrient agar slants at 4 °C.

2.2. Preparation of Cinnamon Extract

The cinnamon powder was suspended in distilled water and heated for approximately 20 min with gentle stirring while being careful not to bring the suspension to a vigorous boil to preserve heat-sensitive constituents, to prepare an aqueous extract. The filtrate was used in the synthesis step after cooling to room temperature and filtering through Whatman No. 1 paper for removal of particulate matter. The freshly made extract had a distinct reddish-brown colour, and a characteristic aroma.

2.3. Synthesis of Selenium Nanoparticles

Sodium selenite was first dissolved in distilled water to form a 1 M precursor solution. The selenite solution was then dropped into the cinnamon extract, a total of 25 mL, while stirring magnetically. The pH of the resulting mixture was followed using a digital pH meter, the ascorbic acid was added dropwise until the pH had reached the near neutral range and here its function was to buffer the medium, not necessarily to be the predominant reductant. Reaction vessel temperature was kept from 60 to 70 °C during the synthesis.

Following a little over a quarter of an hour of being heated with stirring, there was a distinct change in colour - the pale-brown mixture became progressively darker until a full crimson red colour was achieved. The colour change is the visible evidence of the formation of elemental selenium and was considered as the qualitative end-point of the reaction. Heating mantle was then turned off and the suspension was left to cool to room temperature on the bench.

After cooling the solution, an excess of absolute ethanol was then added to precipitate out the colloidal particles. This mixture was put into centrifuge tubes and spun at high speed, and the supernatant was removed and the pellet was washed several times with both distilled water and ethanol to remove unreacted precursor and loosely bound organic residues. After cleaning, the solid was finally dried in an oven at 40 °C to a constant mass to obtain a fine brick red selenium nanoparticles powder. The whole process is summarized graphically in Figure 1.

Figure 1. Step-wise workflow used for the green synthesis of selenium nanoparticles (SeNPs) from sodium selenite and cinnamon bark extract, with ascorbic acid as a pH-buffering agent

2.4. Characterization Techniques

The identity, structure, surface chemistry, morphology, colloidal stability and biological activity of the as-prepared selenium nanoparticles were confirmed using the following techniques.

2.4.1. X-ray Diffraction (XRD)

Powder XRD was used to identify the crystalline phase and to estimate the average crystallite size. Measurements were carried out using Cu Kα radiation (λ = 1.5406 Å). Crystallite size D was estimated from the Debye–Scherrer relation, $D = K\lambda / (\beta \cos \theta)$, where K is the shape factor (taken as 0.9), β is the full-width at half-maximum (FWHM) in radians, and θ is the Bragg angle.

2.4.2. Fourier-Transform Infrared (FTIR) Spectroscopy

FTIR was used to identify the functional groups present at the nanoparticle surface and to infer which classes of biomolecule from the cinnamon extract are involved in reduction and capping. The dried powder was mixed with KBr, pressed into a pellet, and scanned in the 4000–400 cm^{-1} range.

2.4.3. Transmission Electron Microscopy (TEM) and HRTEM

TEM was used to examine particle shape and size distribution, while HRTEM provided lattice-resolved imaging that allowed direct measurement of d-spacings. A drop of dilute aqueous SeNP suspension was deposited on a carbon-coated copper grid and air-dried before imaging. Particle-size statistics were obtained from at least 120 particles using Image.

2.4.4. Zeta Potential Measurement

The surface charge of the colloid was assessed by electrophoretic light scattering. A value of $|\zeta| \geq 30$ mV is generally regarded as the threshold for an electrostatically stable suspension, so this measurement gives a quick indication of the long-term storage behaviour of the product.

2.4.5. Antibacterial Assay (Disc Diffusion)

Kirby–Bauer disc-diffusion method was used to determine antibacterial activity against S. aureus (Gram-positive) and E. coli (Gram-negative) in Mueller–Hinton agar. The SeNP suspension

was placed on the sterile filter-paper discs while sterile distilled water was placed on control discs. After 24 hours of incubation at 37 °C, the inhibitions were measured to the nearest 0.1 mm on the plates. The assays were carried out in triplicate and Student's t-test was used for statistical comparison to the control, at $p < 0.05$. significance.

3. Results and Discussion

3.1. Visual Observation and Formation of SeNPs

During the first few minutes of heating, the reaction mixture had turned from its initial pale colour to progressively through orange and brick shades and ended at a dark crimson red after about 15 minutes heating at 60-70 °C. This colour change is the well-known optical signature of elemental Se produced by the reduction of Se(IV) species, and consistent with the surface plasmon characteristics of nanoscale Se(0) (Forootanfar, et al., 2014; Wadhwani, et al., 2016). Before adding ethanol, there was no turbidity or sedimentation, indicating that the organic shell obtained from cinnamon did not allow the particles to sink at the relatively high concentration of selenium.

3.2. X-ray Diffraction Analysis

The XRD pattern of the dried powder is shown in Figure 2. Nine well-defined Bragg reflections were observed at $2\theta = 23.5°$, 29.7°, 41.3°, 43.6°, 45.4°, 51.7°, 56.1°, 61.8° and 65.3°, and were indexed to the (100), (101), (110), (102), (111), (201), (112), (202) and (210) planes of trigonal selenium (t-Se), in agreement with the standard reference for this phase (ICDD). The (101) reflection at $2\theta \approx 29.7°$ was clearly the most intense, which indicates a preferred orientation along this crystallographic direction. The narrow line widths and low background point to a well-crystallised material with little amorphous content. Indexing parameters and the crystallite size calculated for each reflection are summarised in Table 1.

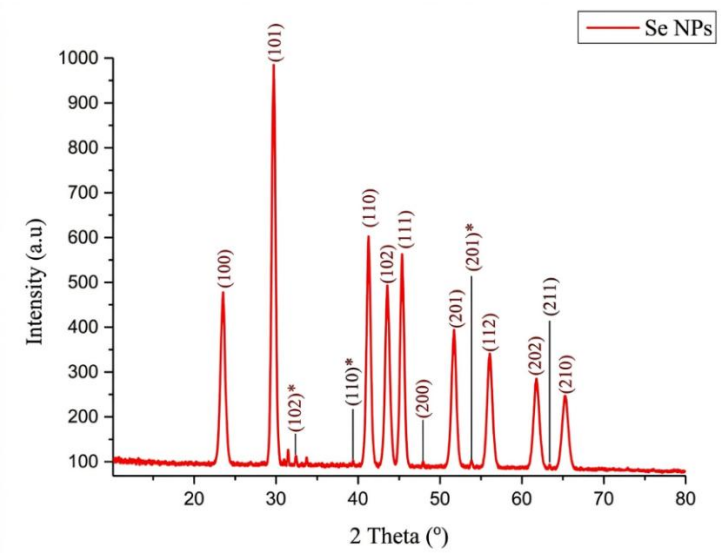

Figure 2. XRD pattern of the as-prepared SeNPs recorded with Cu Kα radiation, with reflections indexed to the trigonal selenium phase.

Table 1. XRD reflection positions, FWHM values, interplanar spacings, Miller indices and crystallite sizes calculated from the Scherrer equation

2θ (°)	FWHM β (°)	d-spacing (Å)	Miller index (hkl)	Crystallite size D (nm)
23.5	0.72	3.7826	(100)	11.27
29.7	0.54	3.0056	(101)	15.22
41.3	0.61	2.1843	(110)	13.92
43.6	0.66	2.0742	(102)	12.96
45.4	0.58	1.9961	(111)	14.85
51.7	0.69	1.7667	(201)	12.79
56.1	0.76	1.6381	(112)	11.84
61.8	0.82	1.5000	(202)	11.29
65.3	0.87	1.4278	(210)	10.85
Average crystallite size				12.78 nm

The crystallite size of the nine reflections is averaged and the mean crystallite size is found to be 12.78 nm. This is a significantly lower average particle size than the one found in the TEM histogram. It is not a contradiction: the size of coherently diffracting domains will be obtained by Scherrer treatment, while TEM will measure the outer envelope of each grain which may include amorphous and/or polycrystalline shell. Thus, a single TEM particle can contain more than one crystallite, especially if capping agents limit the coalescence of grains during nucleation (Patterson, 1939).

3.3. FTIR Analysis and Surface Capping

The FTIR spectrum of the SeNPs is shown in Figure 3. A broad band around 3401 cm-1 corresponds to O–H stretching vibrations of the phenolic and alcoholic groups, which is mostly attributed to the polyphenolic components of the cinnamon extract. The band at 2920 cm-1 is attributed to aliphatic C–H stretching, and the band at 1631 cm-1 is in the region typical of C=O stretching for conjugated carbonyl groups like cinnamaldehyde with possible overlap of C=C ring vibrations of aromatic substructures. The band at 1384 cm–1 could be assigned to C–O stretching and O–H bending and the strong band at 1026 cm–1 was consistent with C–O–C and C–C skeletal vibrations of polyols and ethers (Stuart, 2004). The absorption near 618 cm-1 is assigned to Se–O stretching and is a direct proof that part of the oxygen-containing organic groups is not just co-precipitated with the powder, but is also attached to the surface of the nanoparticles. In conjunction, these characteristics represent an organic corona that is dominated by polyphenolic and aldehydic species, which are precisely the group of functionalities that can be expected to act as electron donors and as steric stabilisers at the same time.

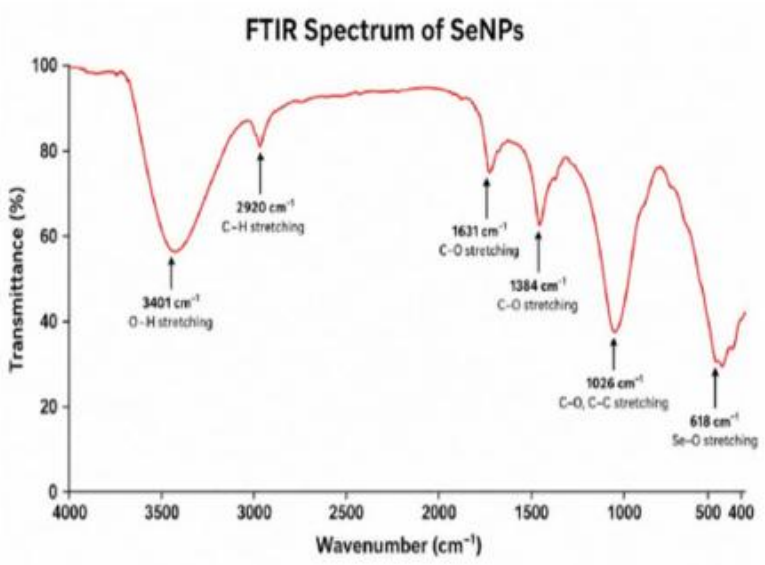

Figure 3. FTIR spectrum of the green-synthesised SeNPs, with band assignments indicating the involvement of polyphenolic and aldehydic groups in the surface capping layer.

3.4. TEM Imaging and Particle Size Distribution

Bright-field TEM micrographs show predominantly quasi-spherical particles with smooth contours, distributed over the supporting grid and only loosely aggregated. The histogram in Figure 4 was constructed from 120 individual particles and is well described by an approximately Gaussian distribution centred at 23.5 nm, with a standard deviation of 4.8 nm. The relatively narrow size dispersion is in keeping with a well-controlled nucleation–growth regime, and is comparable to or better than several reports for SeNPs produced with other plant extracts under similar mild conditions (Husen & Siddiqi, 2014; Sharma, et a., 2014).

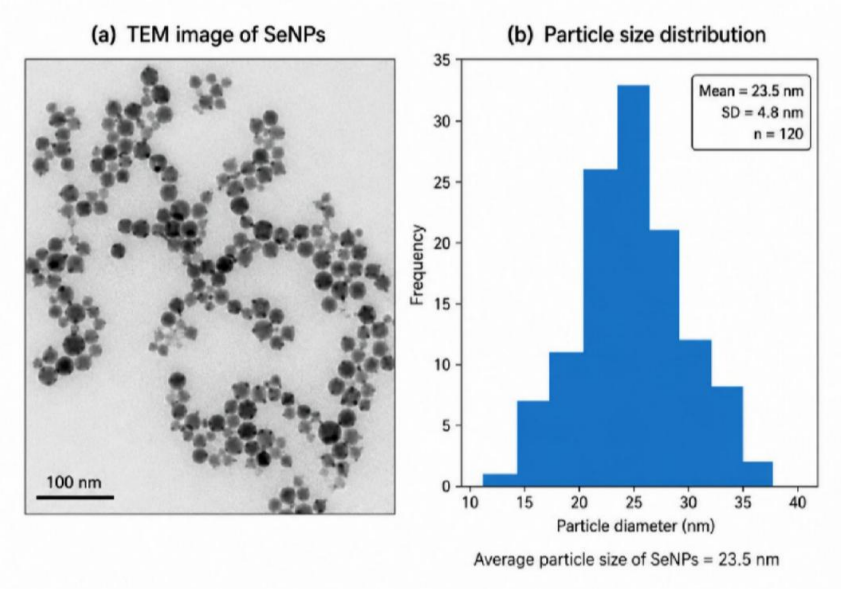

Figure 4. (a) Representative TEM image of the green-synthesised SeNPs and (b) corresponding particle size distribution histogram (n = 120 particles), giving a mean diameter of 23.5 ± 4.8 nm.

3.5. HRTEM and Lattice Analysis

High-resolution imaging was used to verify the crystalline character of the particles and to extract d-spacings directly from the lattice fringes. As shown in Figure 5, well-resolved fringes with an interplanar distance of 0.34 nm were observed across the body of a representative particle, in agreement with the (101) plane of trigonal selenium and consistent with the strongest XRD reflection. Additional sets of fringes corresponding to the (110), (201), (211) and (112) planes were resolved in other particles, with d-spacings of 0.29, 0.20, 0.17 and 0.15 nm respectively. Crystallite sizes derived from these fringe analyses ranged from 11.3 to 13.2 nm, giving an HRTEM-based mean of 12.10 ± 1.01 nm. The agreement between this value and the XRD-derived crystallite size of 12.78 nm obtained on a completely independent footing is one of the more reassuring outcomes of the characterisation.

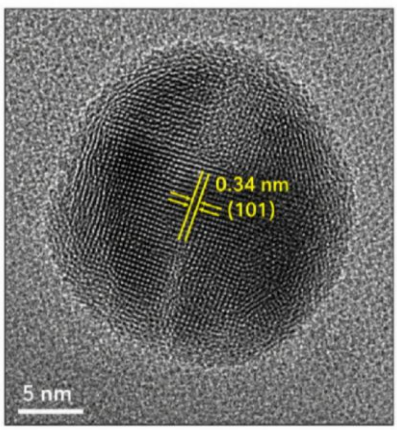

No.	d (nm)	Plane (hkl)	Particle size (nm)
1	0.34	(101)	11.6
2	0.29	(110)	12.4
3	0.20	(201)	13.2
4	0.17	(211)	11.3
5	0.15	(112)	12.0

Average crystallite size (from HRTEM): 12.10 ± 1.01 nm

Figure 5. HRTEM image of a representative SeNP showing the (101) lattice fringe at 0.34 nm; the table on the right lists the d-spacings, indexed planes and crystallite sizes obtained from five particles.

3.6. Colloidal Stability — Zeta Potential

The curve of the zeta potential of the colloid is shown in Figure 6. A single, well-defined peak was detected at −32.4 ± 4.21 mV and a measurement pH of 6.75 with a conductivity of 0.268 mS·cm^{-1}. With aqueous media, the potential measured indicates that the products will have an acceptable shelf life and low flocculating potential when the |ζ| value exceeds 30 mV. The negative sign is consistent

with the surface chemistry deduced from FTIR: deprotonated phenolic and carboxylic groups of the cinnamon-based corona create a net-negative surface, while they also provide the electrosteric repulsions to separate neighbouring particles when they are suspended.

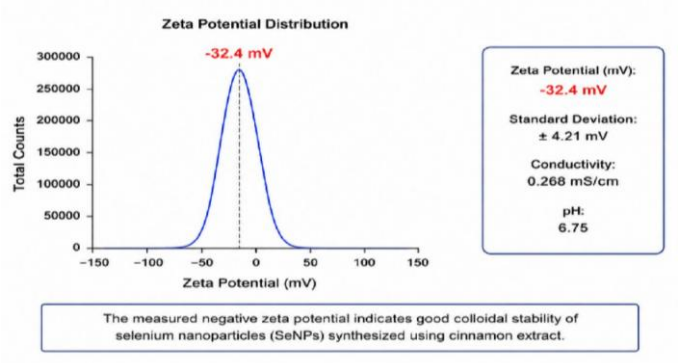

Figure 6. Zeta potential distribution of the SeNP colloid, with a single peak centred at −32.4 mV indicating good electrostatic stability

3.7. Antibacterial Activity

Disc-diffusion plates for the two test organisms are shown in Figure 7. Clear inhibition zones formed around the SeNP-loaded discs in both cases, while the water-loaded control discs produced no measurable zone, ruling out solvent effects. The mean inhibition zone diameter against S. aureus was 18.7 ± 1.2 mm, compared with 14.3 ± 1.0 mm against E. coli (Figure 8). Both values were statistically significant relative to control ($p < 0.001$, Student's t-test, $n = 3$).

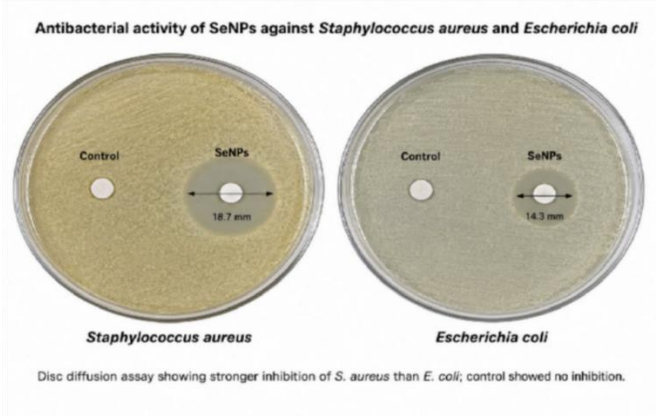

Figure 7. Disc-diffusion assay showing the inhibition zones produced by the cinnamon-mediated SeNPs against (left) Staphylococcus aureus and (right) Escherichia coli; control discs gave no inhibition.

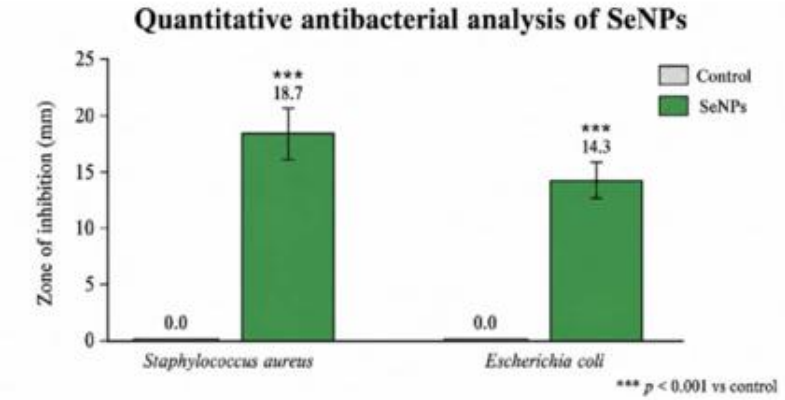

Figure 8. Quantitative comparison of inhibition zones against S. aureus and E. coli (mean ± SD, n = 3); $p < 0.001$ versus control (Student's t-test).

Table 2. Antibacterial activity of selenium nanoparticles (SeNPs) against Staphylococcus aureus and Escherichia coli

Bacterium	Control (mm)	SeNPs (mm)	p-value
Staphylococcus aureus	0.0 0.0	18.7 1.2	< 0.001
Escherichia coli	0.0 0.0	14.3 1.0	< 0.001

Values are mean SD (n = 3). Statistical analysis; Student's t-test versus control.

The greater susceptibility of S. aureus is consistent with what is repeatedly reported for SeNPs and several other metal/metalloid nanoparticles tested against Gram-positive and Gram-negative pairs (Menon, et al., 2018; Vahdati & Tohidi, 2020). The Gram-positive cell wall is dominated by a thick peptidoglycan layer that, although mechanically robust, is also relatively porous and lacks the additional outer membrane that Gram-negative bacteria use as a permeability barrier. Lipopolysaccharide-stabilised outer membranes restrict the access of nano-objects to the periplasmic space and to the cytoplasmic membrane, so a higher local SeNP concentration is normally required to elicit the same response in E. coli. The proposed mechanism of action involves several non-exclusive pathways: generation of reactive oxygen species at the particle surface, direct mechanical and electrostatic disruption of the cell envelope, and slow release of selenium species that interfere with thiol-dependent enzymes (Zonaro, et al., 2015; Khurana, et al. 2019). The negatively charged corona detected by zeta potential measurements does not contradict the picture, because attractive forces at short range can override electrostatic repulsion once a particle is close enough to engage with surface receptors and lipoteichoic acids in the Gram-positive wall.

From a practical standpoint, the inhibition values obtained here compare favourably with those reported for SeNPs prepared by other plant-based routes and tested at comparable doses (Shahverdi, et al., 2007; Khiralla & El-Deeb, 2015), which is encouraging given the simplicity of the synthesis and the food-grade status of cinnamon.

4. Conclusion

Selenium nanoparticles were synthesized in one aqueous step from sodium selenite as precursor and cinnamon (C. zeylanicum) bark extract as main reductant and capping agent, in the presence of a mild pH buffer ascorbic acid. The change in colour was clearly seen as stable crimson, along with the diffraction pattern that was completely attributed to trigonal Selenium, proved the presence of crystalline Se(0). The independent estimates of the crystallite size, obtained from XRD (by Scherrer formula) and from lattice HRTEM analysis, were very close, and the HRTEM revealed quasi-spherical particles with a mean diameter of 23.5 ± 4.8 nm. FTIR analysis indicated the presence of an organic shell of polyphenolic and aldehydic origin at the particle surface, which is in accordance with the zeta potential of -32.4 mV and the colloidal stability of long-term that this figure suggests. In the antibacterial test, the SeNPs gave inhibition zones of 18.7 mm and 14.3 mm against S. aureus and E. coli respectively which were significant compared to control. The low energy synthesis process, ease of use in food, and a well-defined structural and antimicrobial function make cinnamon mediated SeNPs a promising approach for future research with regard to antimicrobial coatings, additives for wound dressings and selenium fortified functional foods. Long-term stability, dose–response curves with a broader range of pathogens and in vitro cytotoxicity assessment on mammalian cell lines will be investigated.

Author Contributions

All authors have equal contributions to the paper. All the authors have read and approved the final manuscript.

Funding

No funding support was received.

Declaration of Conflicting Interests

The author declared no potential conflicts of interest with respect to the research, authorship, and/or publication of this article.

References

Rayman, M. P. (2012). Selenium and human health. *The Lancet, 379*(9822), 1256–1268. https://doi.org/10.1016/S0140-6736(11)61452-9

Papp, L. V., Lu, J., Holmgren, A., & Khanna, K. K. (2007). From selenium to selenoproteins: Synthesis, identity, and their role in human health. *Antioxidants & Redox Signaling, 9*(7), 775–806. https://doi.org/10.1089/ars.2007.1528

Wadhwani, S. A., Shedbalkar, U. U., Singh, R., & Chopade, B. A. (2016). Biogenic selenium nanoparticles: Current status and future prospects. *Applied Microbiology and Biotechnology, 100*(6), 2555–2566. https://doi.org/10.1007/s00253-016-7300-7

Khurana, A., Tekula, S., Saifi, M. A., Venkatesh, P., & Godugu, C. (2019). Therapeutic applications of selenium nanoparticles. *Biomedicine & Pharmacotherapy, 111*, 802–812. https://doi.org/10.1016/j.biopha.2018.12.146

Menon, S., Devi Ks, S., Santhiya, R., Rajeshkumar, S., & Kumar, S. V. (2018). Selenium nanoparticles: A potent chemotherapeutic agent and an elucidation of its mechanism. *Colloids and Surfaces B: Biointerfaces, 170*, 280–292. https://doi.org/10.1016/j.colsurfb.2018.06.006

Tran, P. A., & Webster, T. J. (2011). Selenium nanoparticles inhibit *Staphylococcus aureus* growth. *International Journal of Nanomedicine, 6*, 1553–1558. https://doi.org/10.2147/IJN.S21729

Iravani, S. (2011). Green synthesis of metal nanoparticles using plants. *Green Chemistry, 13*, 2638–2650. https://doi.org/10.1039/C1GC15386B

Mittal, A. K., Chisti, Y., & Banerjee, U. C. (2013). Synthesis of metallic nanoparticles using plant extracts. *Biotechnology Advances, 31*(2), 346–356. https://doi.org/10.1016/j.biotechadv.2013.01.003

Ranasinghe, P., Pigera, S., Premakumara, G. A. S., Galappaththy, P., Constantine, G. R., & Katulanda, P. (2013). Medicinal properties of 'true' cinnamon (*Cinnamomum zeylanicum*): A systematic review. *BMC Complementary and Alternative Medicine, 13*, Article 275. https://doi.org/10.1186/1472-6882-13-275

Sharma, G., Sharma, A. R., Bhavesh, R., Park, J., Ganbold, B., Nam, J.-S., & Lee, S.-S. (2014). Biomolecule-mediated synthesis of selenium nanoparticles using dried *Vitis vinifera* (raisin) extract. *Molecules, 19*(3), 2761–2770. https://doi.org/10.3390/molecules19032761

Khiralla, G. M., & El-Deeb, B. A. (2015). Antimicrobial and antibiofilm effects of selenium nanoparticles on some foodborne pathogens. *LWT - Food Science and Technology, 63*(2), 1001–1007. https://doi.org/10.1016/j.lwt.2015.03.086

Husen, A., & Siddiqi, K. S. (2014). Plants and microbes assisted selenium nanoparticles: Characterization and application. *Journal of Nanobiotechnology, 12*, Article 28. https://doi.org/10.1186/s12951-014-0028-6

Hunter, R. J. (1981). *Zeta potential in colloid science: Principles and applications*. Academic Press.

Forootanfar, H., Adeli-Sardou, M., Nikkhoo, M., Mehrabani, M., Amir-Heidari, B., Shahverdi, A. R., & Shakibaie, M. (2014). Antioxidant and cytotoxic effect of biologically synthesized selenium nanoparticles in comparison to selenium dioxide. *Journal of Trace Elements in Medicine and Biology, 28*(1), 75–79. https://doi.org/10.1016/j.jtemb.2013.07.005

International Centre for Diffraction Data. (n.d.). *Powder diffraction file: Card No. 06-0362, trigonal selenium*. International Centre for Diffraction Data.

Patterson, A. L. (1939). The Scherrer formula for X-ray particle size determination. *Physical Review, 56*(10), 978–982. https://doi.org/10.1103/PhysRev.56.978

Stuart, B. H. (2004). *Infrared spectroscopy: Fundamentals and applications*. John Wiley & Sons. https://doi.org/10.1002/0470011149

Vahdati, M., & Tohidi Moghadam, T. (2020). Synthesis and characterization of selenium nanoparticles-lysozyme nanohybrid system with synergistic antibacterial properties. *Scientific Reports, 10*, Article 510. https://doi.org/10.1038/s41598-019-57333-7

Zonaro, E., Lampis, S., Turner, R. J., Qazi, S. J. S., & Vallini, G. (2015). Biogenic selenium and tellurium nanoparticles synthesized by environmental microbial isolates efficaciously inhibit bacterial planktonic cultures and biofilms. *Frontiers in Microbiology, 6*, Article 584. https://doi.org/10.3389/fmicb.2015.00584

Shahverdi, A. R., Fakhimi, A., Shahverdi, H. R., & Minaian, S. (2007). Synthesis and effect of silver nanoparticles on the antibacterial activity of different antibiotics against *Staphylococcus aureus* and *Escherichia coli*. *Nanomedicine: Nanotechnology, Biology and Medicine, 3*(2), 168–171. https://doi.org/10.1016/j.nano.2007.02.001